Catalysis Today 146 (2009) 223–229

Contents lists available at ScienceDirect

Catalysis Today

journal homepage: www.elsevier.com/locate/cattod

Hydrogen adsorption on model tungsten carbide surfaces

Nicola Gaston *, Shaun Hendy

Industrial Research Limited, Gracefield Research Centre, 69 Gracefield Rd, PO Box 31-310, Lower Hutt 5040, New Zealand

ARTICLE INFO

Article history:
Available online 28 March 2009

Keywords:
Tungsten carbide
Electrocatalysis
Density functional theory
Hydrogen adsorption

ABSTRACT

The potential of tungsten carbide to replace platinum as an anode electrocatalyst has attracted considerable attention due to its activity towards hydrogen oxidation, passivity in acidic electrolyte, and resistance to carbon monoxide poisoning. As a first step towards understanding the mechanisms underlying these qualities, we have performed density functional calculations on slab models of the tungsten carbide surface. We have calculated the adsorption energies of hydrogen on the different available bonding sites, and made a comparison to known values for platinum. The variation of bond strength with surface coverage has been investigated, and used to construct model surface Pourbaix diagrams. The nature and structure of the passivated surface is still an open question. It is possible that the tungsten dissolves out of the top-most surface layers, leaving a surface enriched in carbon. We have studied the effect of additional layers of carbon on the adsorption behaviour of hydrogen. While the most stable surface in its bare form provides binding sites that adsorb carbon with an energy of around 4.0 eV, about 60% higher than the adsorption energy of hydrogen on platinum, a carbonaceous tungsten carbide surface provides a maximum binding energy of 2.49–2.69 eV, much closer to the optimum value for efficient catalysis.

1. Introduction

Hydrogen fuel cells offer the potential for clean and efficient power generation, and are attracting considerable interest for transport applications. One of the principal obstacles to commercialisation is the dependence of current fuel cells on the platinum-group catalysts, which is a practical limitation due to their high cost and scarcity. Non-noble metals are unable to be used in acidic electrolytes for either cathode or anode applications, as they lack the required stability. However metal carbides, in particular tungsten carbide, have promising stability and electrocatalytic activity in acid electrolytes [1–5].

Tungsten carbide is one of the most interesting carbides due to an array of mechanical, electrical, and chemical properties which offer applications in tribology [6–8], microelectronics [9], and heterogeneous catalysis [1]. The superior hardness of tungsten carbide, to which its wear-resistance can be attributed, is related to the particular bonding character of carbides, which can be described as strongly directional due to the interstitial carbon contributing to strong metal–carbon bonds (i.e. strong p- and d-hybridisation), but with an additional contribution to bonding from the original metal–metal bonding in the lattice [10–12]. The characterisation of the carbon atoms as interstitial is supported by the fact that the metal–metal distance in the carbide remains almost unchanged from that of the pure metal. In addition, only the first few groups of the transition metals form stable stoichiometric carbides, with the limiting quantity for stability being the ratio of the carbon to metal atom radii; $R_C/R_M < 0.59$ [7]. However unlike the other transition metal carbides, tungsten carbide does not adopt the rock salt structure where the carbon atoms sit in the interstitial sites of the metal face-centred cubic (fcc) lattice. Instead it forms a hexagonal structure related to the hexagonal close-packed (hcp) structure, in which the ABA stacking consists of WCW stacking in alternating layers of close-packed atoms. The c/a ratio is almost 1, allowing for the carbon atoms to be considered as quasi-interstitial. This structure is clearly unrelated to the body-centred cubic (bcc) structure of tungsten itself.

The platinum-like behaviour of tungsten carbides in the catalysis of hydrogenolysis and isomerisation reactions was discovered by Levy and Boudart [1], and has led to extensive work on the potential of tungsten carbide as an electrocatalyst, due to its stability in acidic solution [3,4]. The effectiveness of tungsten carbide as an electrocatalyst depends crucially on a number of factors, the first of which is that it must be a good electrical conductor. Secondly, it must be highly active for the desired electrocatalytic reaction. Thirdly, it must be passive towards corrosion in the necessary electrolyte. In the case of an anode electrocatalyst, there are very few candidate materials which are both active towards the oxidation of hydrogen and methanol and passive in acidic electrolytes. Moreover, resistance to poisoning by

* Corresponding author.
E-mail address: n.gaston@irl.cri.nz (N. Gaston).

0920-5861/$ – see front matter © 2008 Elsevier B.V. All rights reserved.
doi:10.1016/j.cattod.2008.10.050

carbon monoxide, which is invariably present in either the hydrogen fuel or as a byproduct in the methanol oxidation reaction, is a necessary quality that has been demonstrated for tungsten carbide catalysts [5], and may actually allow for improvement in operating efficiency over current catalysts. In the presence of 100 ppm CO the current densities produced by known Pt/Ru anode catalysts for hydrogen electro-oxidation have been shown to decrease strongly [13].

What structural and chemical changes take place as the tungsten carbide passivates is still a partially open question. Recent experiments [3] showed that the passivity may be due to the formation of a tungsten oxide film, or alternatively, that the tungsten may dissolve from the surface of the carbide to leave a protective carbon layer. From the much greater passivity of WC than W_2C, and the faster oxidation of hydrogen on the WC phase independent of potential, it was concluded that the second scenario is more likely, since the carbon component of the surface appears to be itself necessary for electrocatalysis. Moreover, a small increase in the hydrogen oxidation current is observed at the same time as the corrosion current is in decline, implying that passivation increases electrocatalytic activity. Again, this implies that the passivating carbon has a role to play in the electrocatalysis.

Previous studies [6,14] have shown that for tungsten carbide produced via chemical vapour deposition, oxygen present at the surface does not necessarily imply the presence of tungsten oxide; on the contrary, the oxygen atoms may replace carbon atoms within the lattice of the carbide, as these carbon atoms migrate to the surface to form a carbonaceous layer (of non-carbidic carbon). It is an open question as to whether such a mechanism could be related to the passivation process that takes place in the acidic electrolyte.

In this study we aim to clarify the likely nature of the electrocatalytically active tungsten carbide surfaces and to investigate possible binding sites for hydrogen using density functional theory (DFT). We begin by comparing the experimental results to the bulk cohesive energy and lattice parameters predicted by theory. We then examine the relative stabilities of the tungsten and carbon-terminated (0 0 0 1)-surfaces, before looking at the binding of hydrogen at a variety of sites and surface coverages to these surfaces. We then briefly consider the role of potential and pH in determing surface coverage of hydrogen. Finally we look at the effect of carbonaceous layers on the binding of hydrogen to the (0 0 0 1) surface.

2. Technical details

We perform calculations within the framework of DFT [15] as implemented within the Vienna Ab-initio Simulation Package (VASP) [16–18] with ultrasoft pseudopotentials [19,20]. In this program the Kohn–Sham equations [21] are solved self-consistently for a periodic system, allowing for full three-dimensional translational symmetry in the case of bulk calculations, or slab calculations allowing for two-dimensional translational symmetry of the unit cell with the third dimension incorporating a large volume of vacuum space between cells. The energy cutoff of our plane-wave basis set was increased by 30% from the default, and our Monkhorst–Pack grid contained 231 k-points for the bulk, generated from a $13 \times 13 \times 13$ grid centered on the Gamma point. We first calculated the bulk cohesive energy and lattice parameters in order to compare to experimental data. Results are presented in Table 1. The Perdew–Wang-91 [22] parametrisation of the generalised gradient approximation (GGA) was employed for all slab calculations due to its reliable reproduction of ground state properties for the bulk. The bulk cohesive energy and lattice parameters obtained with DFT are presented in Table 1.

Table 1
The bulk properties of tungsten carbide, as calculated with DFT, and compared with experiment.

Experiment	a (Å)	c (Å)	$E_{cohesive}$ (eV)
	2.907	2.837	16.68
LDA	2.882	2.807	19.57
PBE	2.915	2.839	16.34
PW91	2.919	2.845	16.51

Clearly DFT has little difficulty in describing the ground state properties of tungsten carbide. The local-density approximation is overbinding, as expected, while both commonly used GGA functionals produce both lattice parameters and cohesive energy in very good agreement with experiment. The density of states (DOS) as calculated with GGA-PW91 is shown in Fig. 1. The states at the Fermi level are clearly due to the tungsten d-band, while the carbon s- and p-states lie some way below the Fermi level.

3. Results

3.1. Surface energies

In order to consider the catalytic properties of tungsten carbide, the surface structure needs to be considered. There are three important surface orientations to consider for the tungsten carbide surface: a hexagonal surface (0 0 0 1) which may be either carbon or tungsten terminated, a square (1 $\bar{1}$ 0 0) surface, either carbon or tungsten terminated, and a (2 $\bar{1}$ $\bar{1}$ 0) surface, where there are equal numbers of carbon and tungsten on the surface. In the high-surface area materials that are prepared for use as catalysts, the properties of the most stable surface are liable to be important, in addition to the activity due to surface defects such as steps and edges. The activity and behaviour of the most stable (0 0 0 1) surface [23] is the subject of this work.

The size of the slab used to model the surface is critical to the quality of the calculated energies. We have tested slabs of three different sizes, both of symmetric construction (i.e. terminated by a carbon layer on both sides) and asymmetric (terminated by carbon on one side and tungsten on the other). In all cases one side of the slab was initially relaxed and the results compared for the different

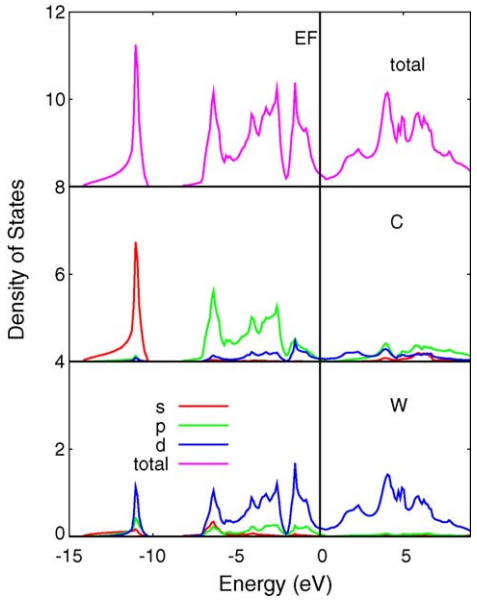

Fig. 1. The PW91 density of states for tungsten carbide. Top: the total DOS; middle: the carbon-projected density of states; bottom: the tungsten-projected DOS.

slabs. A vacuum region of 20 Å was included to avoid interactions between neighbouring slabs. The relaxation energies and distances of the six different model surfaces (both tungsten and carbon terminated) are presented in Table 2.

In the case of the tungsten-terminated surface, relaxation of the surface layer gains little energy, between 0.01 and 0.06 eV for the different models. In the case of the carbon-terminated layers the situation is quite different; relaxation of the carbon surface leads to a gain in energy of between 0.64 and 0.88 eV, in agreement with previously published results [24]. When the underlying tungsten layer is also relaxed, approximately another 0.1 eV is gained. Notably the two asymmetric slabs agree closely on the relaxation energy of the two slabs, at 0.85 or 0.87 eV for the 7- and 9-layer models, respectively; the relaxation energy of the asymmetric slab is 0.06 eV larger, possibly due to slightly larger polarisation effects. These energetic gains for the carbon surface correspond to a contraction of the distance of the surface carbon layer from the bulk of around 0.25 Å, and an additional 0.07 Å shift of the underlying tungsten towards the bulk. The overall relaxation behaviour of the different surfaces is as expected since the dimensions of the lattice are controlled by the size of the tungsten atoms, since the W–W bonds are only slightly longer (2.84 Å) than in bcc tungsten (2.74 Å). The carbon atoms, however, once on the surface and freed from the constraints of the three-dimensional lattice, are able to move further into the threefold tungsten sites, minimising the W–C bond length and gaining binding energy.

The total surface energies of the tungsten and carbon-terminated slabs has been calculated as

$$\sigma = E_{\text{tot}} - \Sigma_i E_{\text{atom}}(i) - nE_{\text{bulk binding}} \quad (1)$$

where n is the number of complete unit cells contained in the bulk, E_{tot} is the total DFT energy for the surface, $E_{\text{atom}}(i)$ are the individual energies of the atoms, and $E_{\text{bulk binding}}$ is the binding energy of the bulk (per unit cell). The tungsten and carbon-terminated (7-layer) slabs then have surface energies of −5.40 and −2.01 eV, respectively. The difference in energy is expected since the binding of tungsten carbide is dominated by the W–W bonding, and therefore it makes sense that the tungsten-terminated surface should be more strongly bound.

3.2. Hydrogen adsorption

There are three different sites for hydrogen adsorption on the carbon-terminated (0 0 0 1) surface, as shown in Fig. 2. The hydrogen adsorption energy is given relative to the energy of atomic hydrogen.

The effect of slab size on the hydrogen adsorption energy has been considered, and the results are presented in Table 3. The largest effect on the calculated adsorption energy is 0.11 eV, or 2%.

Table 2
Relaxation of differently sized models for the tungsten carbide surface. The slabs range from 7 layers to 9 layers deep, either tungsten or carbon terminated, and may be symmetric or asymmetric. 1l indicates the relaxation of one layer, 2l that of two layers. r_1 is the distance that the surface layer or atoms moves towards the slab; r_2 is the relaxation distance of the underlying layer of atoms.

Slab	Carbon terminated			Tungsten terminated		
	3W/4C	4W/4C	4W/5C	3C/4W	4C/4W	4C/5W
E_r (eV)						
1l	−0.79	−0.88	−0.64	−0.01	−0.03	−0.01
2l	−0.85	−0.93	−0.87	−0.03	−0.03	−0.06
R_r (Å)						
1l(r_1)	−0.31	−0.32	−0.17	−0.10	−0.05	−0.06
2l(r_1)	−0.24	−0.26	−0.24	−0.04	−0.04	−0.04
2l(r_2)	−0.08	−0.07	−0.06	−0.02	−0.03	−0.02

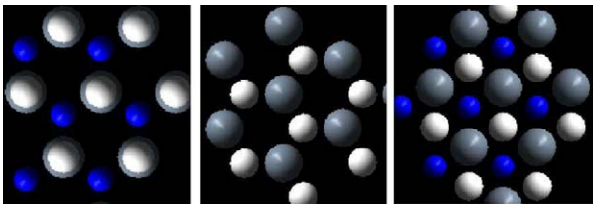

Fig. 2. From left to right, the top, hollow threefold (with ABA stacking) and hollow (ABC) sites are shown. The white atoms are hydrogen, sitting on top of alternating layers of tungsten (blue) and carbon (grey) atoms. (For interpretation of the references to color in the figure caption, the reader is referred to the web version of the article.)

Table 3
Convergence of the hydrogen adsorption energies with respect to slab size. The adsorption energy E_H, hydrogen bond length R_H, and vertical distance of hydrogen from the surface R_V are given.

Size of slab	3W/4C	4W/4C	4W/5C	3C/4W	4C/4W	4C/5W
E_H (eV)						
Top	−4.51	−4.40	−4.48	−2.91	−2.87	−2.89
ABA	−2.82	−2.83	−2.84	−3.88	−3.86	−3.89
ABC	−2.33	−2.35	−2.35	−4.05	−4.09	−4.12
R_H (Å)						
Top	1.126	1.057	1.075	1.565	1.565	1.566
ABA	1.783	1.787	1.781	2.001	2.002	2.001
ABC	1.701	1.711	1.712	1.962	1.979	1.988
R_V (Å)						
Top	1.126	1.057	1.075	1.565	1.565	1.566
ABA	0.580	0.570	0.578	1.086	1.081	1.097
ABC	0.233	0.265	0.261	1.048	1.043	1.054

In terms of hydrogen bond lengths, the largest difference is 0.07 Å, or 6%. The smallest slab model overestimates the binding to the on-top site when compared to the larger slabs, but slightly underestimates the binding to the threefold hollow sites. Overall the error introduced by using the smallest of the three slab models appears negligible when compared with the expected accuracy of DFT. Furthermore, the slab thickness does not significantly alter the relative stability of the three binding sites: on the carbon-terminated surface, the top sites are preferred, whereas on the tungsten-terminated surface, the ABC sites are preferred. In all further calculations we consider only the 7-layer slab (either tungsten or carbon terminated). The calculated adsorption properties of hydrogen on the WC (0 0 0 1) 7-layer surface are summarised in Table 4.

3.3. Coverage dependence of adsorption

The effect of surface coverage on the adsorption energy of atomic hydrogen has been investigated. We have considered coverages ranging from a 0.25 monolayer (ML) to 1.0 ML of

Table 4
Adsorption energies and bond lengths for hydrogen atoms on the tungsten carbide surface.

	Top	ABC	ABA
Carbon terminated			
Adsorption energy (eV)	−4.51	−2.33	−2.82
H–C distance (Å)	1.126	1.701	1.783
Out of plane H-distance (Å)	1.126	0.233	0.580
Tungsten terminated			
Adsorption energy (eV)	−2.91	−4.05	−3.88
H–W distance (Å)	1.565	1.962	2.001
Out of plane H-distance (Å)	1.565	1.048	1.086

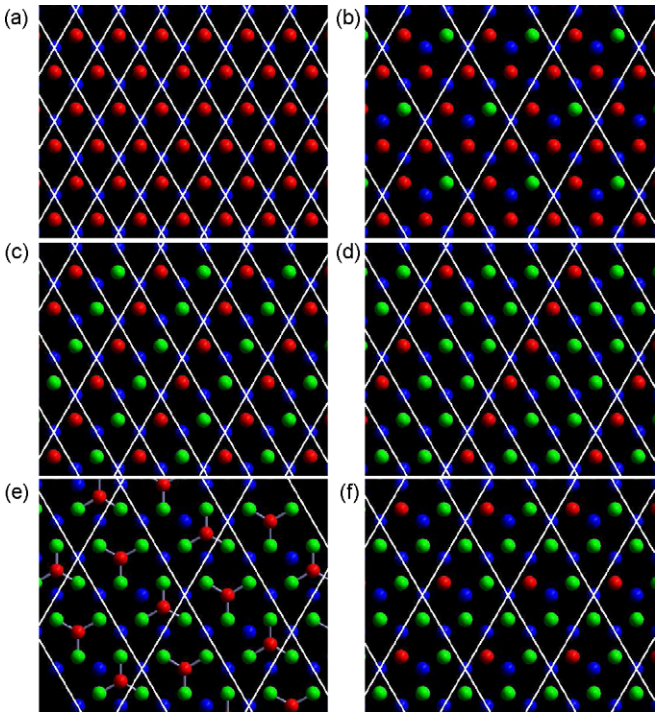

Fig. 3. The coverage models considered. All pictures except (e) are drawn with the hydrogen (red) adsorbing on the on-top site (over the green atoms) with the below-surface layer represented by dark blue atoms. (a) 1 ML coverage; (b) 0.75 ML coverage (2 × 2) model; (c) 0.5 ML coverage (2 × 1) model; (d) 0.33 ML coverage, (3 × 1) model; (e) 0.33 ML coverage (3 × 2) model (mixed ABA and ABC sites); (f) 0.25 ML coverage (2 × 2) model. The unit cells are marked with white lines. (For interpretation of the references to color in the figure caption, the reader is referred to the web version of the article.)

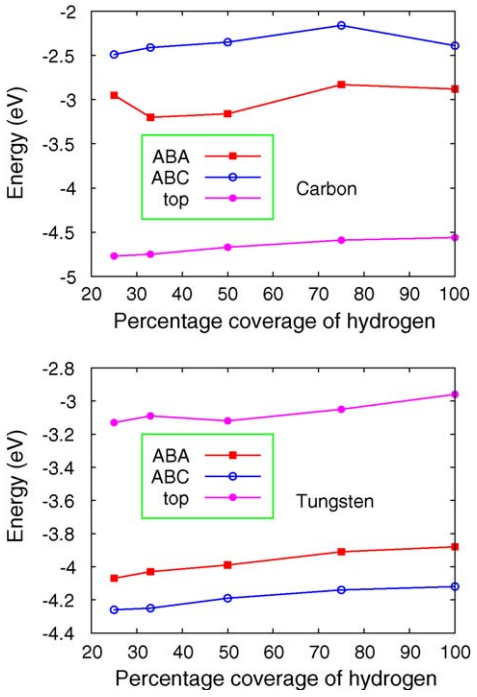

Fig. 4. The effect of coverage on the adsorption energy of atomic hydrogen on a 7-layer slab. Above, a carbon-terminated slab; below, tungsten terminated.

hydrogen atoms, with a range of unit cell models. The coverage models considered are presented in Fig. 3.

The calculated absorption energies for the carbon and tungsten-terminated surfaces are shown in Fig. 4 as a function of coverage of each of the three absorption sites. As is usual for hydrogen adsorption, there is generally weak repulsion between the adsorbed atoms, leading to a decrease in adsorption energy with coverage. The magnitude of the total effective repulsion is relatively small in all cases, when compared to the sensitivity of the binding energy to adsorption site. The total energy change over the range 25–100% coverage is around 0.3 eV for the carbon-terminated surfaces, and close to half that amount for the tungsten-terminated surfaces. For the carbon-terminated surfaces there is an increase in the binding energy upon going from 0.25 to 0.33 ML coverage on the threefold sites, before a subsequent decrease with increased coverage.

Since the lattice spacing is reasonably large relative to the H_2 bond length, the direct H–H repulsion is too small to account for the magnitude of the coverage dependence seen here. This may be demonstrated by the comparison of two models for 0.33 ML coverage, one of which (Fig. 3d) uses a (3 × 1) cell, and the other (Fig. 3e) a (3 × 2) cell. By allowing occupancy of both ABC and ABA-type threefold sites in the second case, the shortest distance between the hydrogen atoms is increased to 4.03 Å from the nearest neighbour value of 2.92 Å, minimising direct repulsion for the same coverage value. However, the adsorption energy is barely affected by the nearest neighbour distance. For the tungsten-terminated surface the adsorption energy of hydrogen on the mixed ABA/ABC surface ($r_{HH} = 4.03$ Å) is 4.14 eV, exactly the average of the values on the separate surfaces at the same coverage (4.03 eV for the ABA site, 4.25 eV for the ABC site). For the carbon-terminated surface the mixed 0.33 ML surface has an adsorption energy of 2.67 eV, compared to 3.20 (ABA) and 2.41 (ABC). Therefore the coverage dependence of the hydrogen adsorption energy seems to be indirectly repulsive rather than dependent on H–H distance; i.e. it is mediated by the surface.

3.4. Surface Pourbaix diagrams

The most stable surfaces are determined using the theoretical standard hydrogen electrode (SHE) [25,26] and used to construct Pourbaix diagrams. The adsorption of hydrogen atoms on the surface can be written as

$$(1/2)H_2(g) \rightarrow H^* \quad (2)$$

which is followed by desorption of protons into the electrolyte:

$$H^* \rightarrow H^+ + e^-. \quad (3)$$

The SHE is defined such that the reaction

$$(1/2)H_2(g) \rightarrow H^+ + e^-, \quad (4)$$

has a reaction free energy $\Delta G_0 = 0$ at a potential $U = 0$ V, at standard conditions (pH 0, p (H_2) = 1 bar, T = 298 K). Thus as the potential is changed the chemical potential of the rhs of Eq. (4) changes by $-eU$ with respect to H_2 in the gas phase. If we consider the Born–Haber cycle $(1/2)H_2(g) \rightarrow H^* \rightarrow H^+ + e^-$, we can relate the ΔG of Eq. (3) to the electrode potential via

$$\Delta G = -(\Delta G_0 + eU_{SHE}). \quad (5)$$

and

$$\Delta G_0 = \Delta E - T\Delta S. \quad (6)$$

The ΔE here is the calculated DFT energy for Eq. (2), which we correct for the effects of entropy to obtain the free energy ΔG_0. The change in entropy, ΔS, includes the gain of translational degrees of freedom during desorption to H^+, which may be taken from standard tables [27], as well as the configurational entropy change

which depends on coverage Θas

$$\Delta S_{\text{conf}} = k_B \ln\left(\frac{1-\Theta}{\Theta}\right). \quad (7)$$

This means that as we increase the potential, the barrier to H^+ desorption decreases. Since this decrease depends on coverage, there is a transition from low coverages being preferred at low (negative) potentials, to higher coverages being preferred at more positive potentials. The effect of pH is to shift the free energy of the desorption process by $-k_B T \ln 10 \text{pH}$, which at 298 K produces lines of a slope −0.059 eV/pH. This means that at low pH there will be a lower barrier to desorption of H^+, and an associated increase of stability of the low coverage surfaces (at negative potentials).

The actual charge transfer associated with the desorption process depends on the amount of charge transferred during the adsorption reaction, Eq. (2), i.e. we take the actual charge transferred to be

$$CT_{\text{desorption}} = 1 - CT_{\text{adsorption}} \quad (8)$$

where $CT_{\text{adsorption}}$ is taken from our DFT calculations. For this we rely on the 'atoms-in-molecules' approach to defining atomic charge [28], calculated using the Bader charge analysis code [29,30] which divides charge density into atomic charges separated by minima in the charge density. This charge varies with both coverage and binding site of the adsorbed hydrogen, as shown in Fig. 5. For adsorption on the tungsten-terminated surface, there is always a net negative charge on the hydrogen atom. The amount of charge transferred for the different adsorption sites correlates directly with the ordering of the preferred adsorption sites, as shown in Fig. 4. This clear relationship does not hold for the case of the carbon-terminated surfaces, and the weakly non-monotonic behaviour of the adsorption energies is much more strongly visible in the plots of transferred charge against coverage. However the absolute amount of charge transferred is much weaker in the case of the carbon-terminated surfaces, which makes these small changes less meaningful, and it is reasonable to conclude simply that the maximum in the amount of charge transferred at a coverage of 0.33 ML seems to correlate approximately with the minimum in the adsorption energy seen in Fig. 4. Thus the same arguments applied above to the coverage dependence of the adsorption energy seem also to apply to the coverage dependence of the charge transfer; i.e. the indirect nature of the H–H repulsion on the surface will be related to the amount of charge that is able to be accepted by the surface atoms, which appears to saturate at a coverage of 0.33 ML. For example, the on-top site at 1 ML coverage allows transfer of 0.04e to the carbon atom from the hydrogen, but in the case of the tungsten-terminated surface, charge is transferred in the opposite direction, with a net 0.47e being transferred to the hydrogen atom. Therefore the actual slope of the potential dependence in the Pourbaix diagram needs to be calculated in consideration of the fact that 0.96e is being transferred in the reaction of Eq. (3) for the 1 ML carbon-terminated surface, whereas for the tungsten-terminated surface, 1.47e must be transferred to the surface, leading to a much greater potential dependence. This implies that Eq. (5) becomes (with the substitution of Eq. (6) also):

$$\Delta G = -(\Delta E - T\Delta S + CT_{\text{desorption}} e U_{\text{SHE}}). \quad (9)$$

The pH dependence is unchanged by this consideration, since only one proton per hydrogen atom can be released. The Pourbaix diagrams for the most stable surfaces as functions of potential (SHE) and pH, with respect to the desorption of protons from the different surfaces are presented in Fig. 6. The experimentally observed threshold for the breakdown of passivation [3] is marked on the Pourbaix diagrams at a potential value independent of pH. Since we can consider the overall reaction associated with this as

$$WC(s) \rightarrow C(s) + W^{4+}(aq) + 4e^-, \quad (10)$$

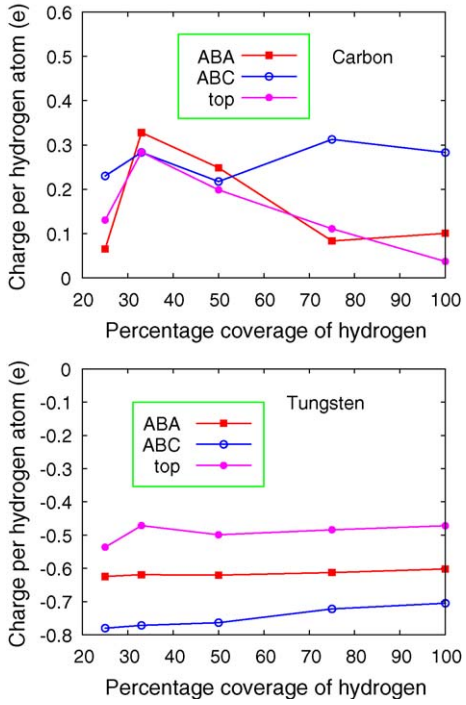

Fig. 5. The effect of coverage on the charge transfer between hydrogen and the surface on a 7-layer slab. Above, a carbon-terminated slab; below, tungsten terminated.

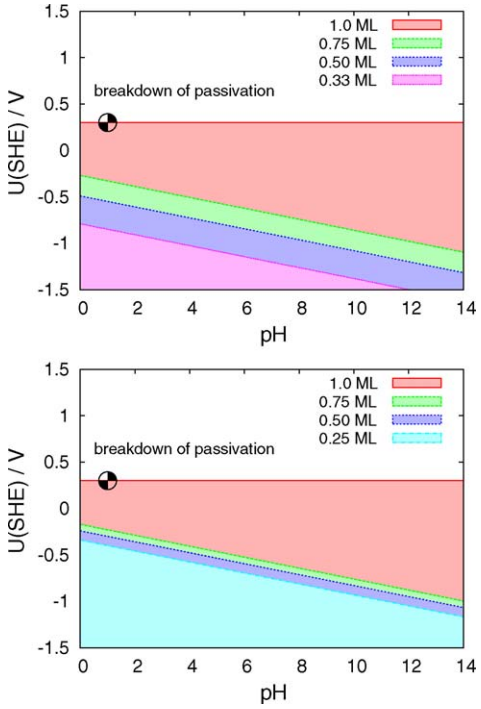

Fig. 6. Pourbaix diagrams for the carbon (top) and tungsten (below) terminated surfaces, using the calculated values of charge transfer per adsorbed hydrogen atom. The experimentally observed onset of breakdown of passivity at 0.3 V (SHE) at low pH is marked. Typical operating conditions of a fuel cell anode for hydrogen oxidation would be at low pH, and high positive potentials.

the overall reaction can be said to depend on potential due to the exchange of electrons, but does not depend on pH as there are no protons involved. In reality, the mechanism of corrosion of the W atoms into solution will be different in different electrolytes and at different pH, but this is beyond the scope of the current work. Between the threshold for the breakdown of passivation and zero potential, it can be seen from the Pourbaix diagrams that the barrier to desorption of H^+ will be minimised for 1.0 ML coverage of either the tungsten or carbon-terminated surfaces, for potentials relevant for oxidation of hydrogen.

3.5. The effect of surface carbon

The adsorption energy of hydrogen on Pt, Rh, or Ir, the metals which sit at the top of a volcano plot of $\log(i_0)$ vs. M–H bond strength, is about 2.6 eV. Above or below this value of the binding energy, a marked decrease in anodic hydrogen oxidation current densities is observed. If we consider this an optimum value of the binding energy, or a range of 2.4–2.8 eV (bulk W binds hydrogen by 2.9 eV) then it seems that the W–H bond either on the surface or the underlying layer still comes closest to this value, at 2.90 and 2.81 eV, respectively. However it is not clear that the adsorption energy on clean sites is the critical factor in determining the activity of the catalyst.

One hypothesis that fits the experimental observation of passivation in acid being accompanied by an increased catalytic activity, is that the metal atoms near the surface are indeed dissolved by the acid as part of the passivation process. This would leave behind a carbonaceous layer at the surface, upon which the catalytic activity would occur. To test this model of the passivation process, we have calculated the adsorption energy of hydrogen atoms on carbon-enriched versions of the 7-layer tungsten carbide model described above. Surprisingly, the first layer of additional carbon binds just as strongly to the slab as the previous layer of carbon (the per-atom cohesive energy of the slab stays constant). Adding a third and fourth layer of carbon atoms decreases the per-atom cohesive energy of the slab by (successively) 0.14 and 0.12 eV, respectively (a decrease of about 2% per layer).

The overall effect of the additional layers of carbon is to decrease the adsorption energy of hydrogen. The adsorption energies are plotted in Fig. 7 as a function of the amount of surface carbon. Each additional layer of carbon has continued the ABA stacking of the WC lattice. It is therefore not particularly surprising that the additional layers of carbon intercalate, forming a rough graphene bilayer once there are four carbon layers on the underlying tungsten (0 0 0 1) surface. The resulting carbon–carbon distance in such an arrangement is 1.68 Å, with each hexagonal ring centred on a tungsten atom. Due to the enforced lengthening of the carbon–carbon bond from the graphitic value (1.42 Å), this film may be considered rather reactive, and shows similar properties to that of "reactive" epitaxial graphene films on, for example, TaC surfaces [31]. As a consequence the graphene sheet is distorted from planarity by about 0.2–0.3 Å, with the innermost sheet more strongly distorted by interactions with the underlying substrate (this distortion is apparent even in the absence of the adsorbed hydrogen atoms). Whereas the effect of a single layer of carbon is to increase the maximum binding energy considerably when compared to the tungsten-terminated surface, additional layers of carbon decrease this energy, that of the on-top adsorbed hydrogen atom, by around 1 eV per layer of carbon for the next two layers. At four layers of carbon, the effect appears to have saturated. It is important to note that the single layer of carbon corresponds to carbidic carbon, while the additional layers of carbon become increasingly graphitic in nature. Thus the decreased adsorption energy with increasing layers of carbon may be thought of as simply due to the improved carbon–carbon bonding which reduces the ability of carbon to subsequently bond to the adsorbing hydrogen atoms. While this is a simple model for the structure of additional carbon at the surface of WC, the underlying hcp-like tungsten carbide structure makes it rather plausible. Subsequent reconstruction of the carbon-terminated surface is possible, and even probable, but since mono- and bi-layers of graphene on incommensurate surfaces (such as TaC (1 1 1) [31]) are known, the final structure may be not dissimilar to those considered here.

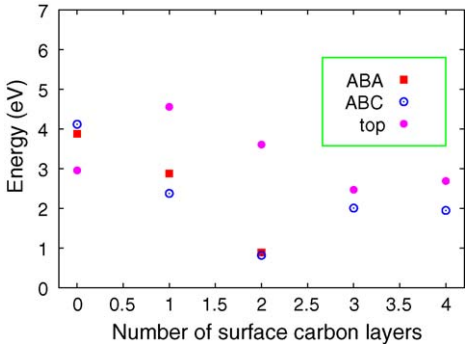

Fig. 7. The effect of surface carbon on the adsorption energy of atomic hydrogen at on-top, threefold ABA, and ABC type sites.

After three or four layers of carbon are considered, the maximum binding energy of the hydrogen atom to the on-top position has been reduced to 2.49 and 2.69 eV, respectively. The threefold ABA site then has essentially the same binding energy, since the A- and B-layers of carbon atoms have closely merged. Thus the effective binding energy of hydrogen to the carbon rich tungsten carbide surface is very close to the approximately 2.6 eV of hydrogen adsorbed on platinum.

4. Conclusions

DFT calculations have been used to describe the adsorption process of hydrogen on model tungsten carbide surfaces. Both the adsorption energies and partial charges of the adsorbed hydrogen atoms depend strongly on the surface termination (carbon or tungsten) and the nature of the binding site; the observed dependence on coverage is weaker. The coverage dependence of both the energies and charges is non-monotonic for certain of the carbon-terminated bonding sites. Surface Pourbaix diagrams based on the most stable adsorbed species have been constructed for the desorption of H^+ as a function of pH and potential. Partial charges for the adsorbed hydrogen atoms have been used to determine the potential dependence of desorption. For physically relevant potentials for the oxidation of hydrogen, the barrier to desorption of H^+ is minimised for 1.0 ML coverage of hydrogen.

By adding additional layers of carbon to the WC surface, we have shown that the barrier to desorption of hydrogen can be lowered. This is in agreement with the experimental observation that the electrocatalytic activity of the WC material is enhanced by passivation. Thus the hypothesis that the dissolution of tungsten from the tungsten carbide surface during passivation leaves behind a carbon-rich surface of enhanced activity, is consistent with the DFT calculations presented here.

Acknowledgements

We would like to thank Prof. G.T. Burstein for useful discussions. We acknowledge funding from the New Zealand Foundation for Research, Science and Technology, under contract numbers C08X0409 and IRLX0701.

References

[1] R.B. Levy, M. Boudart, Science 181 (1973) 547.
[2] E.C. Weigert, M.B. Zellner, A.L. Stottlemyer, J.G. Chen, Top. Catal. 46 (2007) 349–357.
[3] C.D.A. Brady, E.J. Rees, G.T. Burstein, J. Power Sources 179 (2008) 17–26.
[4] R. Ganesan, D.J. Ham, J.S. Lee, Electrochem. Commun. 9 (2007) 2576–2579.
[5] D.R. McIntyre, G.T. Burstein, A. Vossen, J. Power Sources 107 (2002) 67–73.
[6] K.A. Beadle, R. Gupta, A. Mathew, J.G. Chen, B.G. Willis, Thin Solid Films 516 (2008) 3847–3854.
[7] E.I. Isaev, S.I. Simak, I.A. Abrikosov, R. Ahuja, Yu.Kh. Vekilov, M.I. Katsnelson, A.I. Lichtenstein, B. Johansson, J. Appl. Phys. 101 (2007) 123519.
[8] H.W. Hugosson, H. Engqvist, Int. J. Ref. Met. Hard Mater. 21 (2003) 55–61.
[9] Y.-M. Sun, S.Y. Lee, A.M. Lemonds, E.R. Engbrecht, S. Veldman, J. Lozano, J.M. White, J.G. Ekerdt, I. Emesh, K. Pfeifer, Thin Solid Films 397 (2001) 109.
[10] S.-H. Jhi, J. Ihm, S.G. Louie, M.L. Cohen, Nature 399 (1999) 132–134.
[11] A.Y. Liu, R.M. Wentzcovitch, M.L. Cohen, Phys. Rev. B 38 (1988) 9483–9489.
[12] J.C. Grossman, A. Mizel, M. Coté, M.L. Cohen, S.G. Louie, Phys. Rev. B 60 (1999) 6343–6347.
[13] G.J.K. Acres, J.C. Frost, G.A. Hards, R.J. Potter, T.R. Ralph, D. Thompson, G.T. Burstein, G.J. Hutchings, Catal. Today 38 (1997) 393.
[14] N. Liu, S.A. Rykov, J.G. Chen, Surf. Sci. 487 (2001) 107.
[15] P. Hohenberg, W. Kohn, Phys. Rev. 136 (1964) 864.
[16] G. Kresse, J. Hafner, Phys. Rev. B 47 (1993) 558, ibid. 49 (1994) 14251.
[17] G. Kresse, J. Furthmller, Comput. Mater. Sci. 6 (1996) 15.
[18] G. Kresse, J. Furthmller, Phys. Rev. B 54 (1996) 11169.
[19] G. Kresse, J. Hafner, J. Phys.: Condens. Matter 6 (1994) 8245.
[20] G. Kresse, D. Joubert, Phys. Rev. B 59 (1999) 1758.
[21] W. Kohn, L.J. Sham, Phys. Rev. 140 (1965) 1133.
[22] J.P. Perdew, Y. Wang, Phys. Rev. B 45 (1992) 13244.
[23] N. Juslin, P. Erhart, P. Träskelin, J. Nord, K.O.E. Henriksson, E. Salonen, K. Nordlund, K. Albe, J. Appl. Phys. 98 (2005) 123520.
[24] F. Marinelli, A. Jelea, A. Allouche, Surf. Sci. 601 (2007) 578–587.
[25] H.A. Hansen, J. Rossmeisl, J.K. Nørskov, Phys. Chem. Chem. Phys. 10 (2008) 3722–3730.
[26] G.S. Karlberg, T.F. Jaramillo, E. Skúlason, J. Rossmeisl, T. Bligaard, J.K. Nørskov, Phys. Rev. Lett. 99 (2007) 126101.
[27] D.R. Lide (Ed.), CRC Handbook of Chemistry and Physics, CRC Press, New York, 2002.
[28] R. Bader, Atoms in Molecules: A Quantum Theory, Oxford University Press, New York, 1990.
[29] G. Henkelman, A. Arnaldsson, H. Jónsson, Comput. Mater. Sci. 36 (2006) 254–360.
[30] E. Sanville, S.D. Kenny, R. Smith, G. Henkelman, J. Comp. Chem. 28 (2007) 899–908.
[31] C. Oshima, A. Nagashima, J. Phys.: Condens. Matter 9 (1997) 1–20.